26. G. Kaim, F. Wehrle, U. Gerike, P. Dimroth, *Biochemistry* **36**, 9185 (1997).
27. T. Murata *et al.*, *J. Biol. Chem.* **278**, 21162 (2003).
28. H. Arai *et al.*, *J. Biol. Chem.* **263**, 8796 (1999).
29. A. Holzenburg *et al.*, *Eur. J. Biochem.* **213**, 21 (1993).
30. R. W. Hendrix, *Proc. Natl. Acad. Sci. U.S.A.* **75**, 4779 (1978).
31. D. R. Thomas, D. G. Morgan, D. J. DeRosier, *Proc. Natl. Acad. Sci. U.S.A.* **96**, 10134 (1999).
32. Single-letter abbreviations for the amino acid residues are as follows: A, Ala; C, Cys; D, Asp; E, Glu; F, Phe; G, Gly; H, His; I, Ile; K, Lys; L, Leu; M, Met; N, Asn; P, Pro; Q, Gln; R, Arg; S, Ser; T, Thr; V, Val; W, Trp; and Y, Tyr.
33. J. D. Thompson, D. G. Higgins, T. J. Gibson, *Nucleic Acids Res.* **22**, 4673 (1994).
34. This work was supported by the Medical Research Council. T.M. was supported partly by a Fellowship for Research Abroad from the Japan Society for the Promotion of Science. We thank the staff at the European Synchrotron Radiation Facility in Grenoble for their help. Coordinates and structure factors (accession codes 2bl2 and r2bl2sf) have been deposited in the Protein Data Bank.

Supporting Online Material
www.sciencemag.org/cgi/content/full/1110064/DC1
Materials and Methods
SOM Text
Fig. S1
References

21 January 2005; accepted 8 March 2005
Published online 31 March 2005;
10.1126/science.1110064
Include this information when citing this paper.

Structure of the Rotor Ring of F-Type Na^+-ATPase from *Ilyobacter tartaricus*

Thomas Meier,[1] Patrick Polzer,[2] Kay Diederichs,[2]* Wolfram Welte,[2] Peter Dimroth[1]*

In the crystal structure of the membrane-embedded rotor ring of the sodium ion–translocating adenosine 5′-triphosphate (ATP) synthase of *Ilyobacter tartaricus* at 2.4 angstrom resolution, 11 c subunits are assembled into an hourglass-shaped cylinder with 11-fold symmetry. Sodium ions are bound in a locked conformation close to the outer surface of the cylinder near the middle of the membrane. The structure supports an ion-translocation mechanism in the intact ATP synthase in which the binding site converts from the locked conformation into one that opens toward subunit a as the rotor ring moves through the subunit a/c interface.

In the F_1F_o ATP synthase, the cytoplasmic F_1 catalytic domain (subunits $\alpha_3\beta_3\gamma\delta\varepsilon$) is linked by means of a central and a peripheral stalk (subunits γ/ε and b_2/δ, respectively) to the intrinsic membrane domain called F_o (subunits $ab_2c_{10\text{-}14}$). Each of these domains functions as a reversible rotary motor and exchanges energy with the opposite motor by mechanical rotation of the central stalk. During ATP synthesis, energy stored in an electrochemical gradient of protons or Na^+ ions fuels the F_o motor, which causes the stalk to rotate with the inherently asymmetric γ subunit acting as a camshaft to continuously change the conformation of each catalytic β subunit. These sequential interconversions, which result in ATP synthesis, endow the binding sites with different nucleotide affinities [for reviews see (*1*–*3*)]. The rotational model, which explains a wealth of biochemical and kinetic data, is impressively supported by the crystal structure of F_1 (*4*) and was experimentally verified by biochemical, spectroscopic, and microscopic techniques (*5*).

The F_o motor consists of an oligomeric ring of c subunits that is abutted laterally by the a and b_2 subunits (*6*). The c ring, together with γ/ε subunits, forms the rotor assembly, which spins against the stator components $ab_2\delta\alpha_3\beta_3$. Ion translocation at the interface between subunit a and the c ring, driven by the ion motive force, is thought to generate torque (*7*–*10*) applied to the γ subunit, which is then used to promote the conformational changes required for ATP synthesis at the F_1 catalytic sites.

Despite intense efforts, little is known about the structural details of F_o. This lack of information hinders our understanding of how this molecular motor functions. The nuclear magnetic resonance (NMR) structures of the c monomer of *Escherichia coli* (*7*, *11*) showed that the protein is folded into two α helices linked by a loop. Other structural studies indicated that the c subunits of the oligomer are tightly packed into two concentric rings of helices (*12*, *13*). The number of c monomers per ring varies between n = 10, 11, and 14 units in the ATP synthases from yeast (*12*), *I. tartaricus* (*13*), and spinach chloroplasts (*14*), respectively.

Structure of the c ring. We chose to determine the crystal structure of the *I. tartaricus* c ring because of its inherent stability and relative ease of isolation (*15*). After purification and crystallization of wild-type c ring (*16*), the structure was solved (table S1) by molecular replacement (*17*) using a medium-resolution (6 Å) c-ring backbone model derived from electron crystallography (*13*). The asymmetric unit of the crystal contains 4 c rings. These rings are arranged in two parallel, but laterally translated, c-ring dimers each formed by a coaxial association of two rings that interact with their termini in a tail-to-tail fashion. A non-crystallographic symmetry restraint was imposed during refinement at 2.4 Å over the 44 monomers in the asymmetric unit (3916 residues) with the exclusion of the loop regions that form crystal contacts, which substantially improved the electron density and resulted in an atomic model without Ramachandran plot outliers.

The electron density map of a single c ring shows a cylindrical, hourglass-shaped protein complex of ~70 Å in height, and with an outer diameter of ~40 Å in the middle and ~50 Å at the top and bottom. Eleven c subunits, each composed of two membrane-spanning α helices forming a hairpin, are arranged around an 11-fold axis, creating a tightly packed inner ring with their N-terminal helices (Fig. 1). The C-terminal helices pack into the grooves formed between N-terminal helices, producing an outer ring, in agreement with previous medium-resolution structures (*12*, *13*). In the electron density map, the backbone and side chains of all amino acids are clearly defined, except for the C-terminal glycine. The N- and C-terminal helices are connected by a loop formed by the highly conserved peptide Arg^{45}, Gln^{46}, and Pro^{47}, which is exposed to the cytoplasmic surface (Fig. 2) (*18*, *19*). The chain termini are exposed to the periplasm.

The C-terminal helices are shorter than the N-terminal helices, owing to a break at Tyr^{80} followed by another short helix of one turn (Figs. 1 and 2). For each helix, an individual plane can be found that roughly contains the axis of the helix and the c-ring symmetry axis (Fig. 1A). All helices show a bend of about 20° in the middle of the membrane (at Pro^{28} and Glu^{65} in the N-terminal and the C-terminal helices, respectively), causing the narrow part of the hourglass shape. Moreover, the bend tilts the helices in the cytoplasmic half out of the plane by ~10°, yielding a right-handed twisted packing (Fig. 1A). When the c ring is viewed from the cytoplasm, it rotates counterclockwise during ATP synthesis (*20*) against the drag imposed by the F_1 motor components. Thus, the resulting torque might decrease the bend and increase the interhelical distance in the cytoplasmic part of the c ring, depending on the energies involved. Such a conformational change under load might serve to store elastic energy in the c ring, adding to that described for the central and peripheral stalk subunits (*21*). A change in the twist of the helices is supported by calculations (*22*) that show in the lowest-order mode a torsional

[1]Institut für Mikrobiologie, Eidgenössische Technische Hochschule (ETH), Zürich Hönggerberg, Wolfgang-Pauli-Str. 10, CH-8093 Zürich, Switzerland. [2]Fachbereich Biologie, Universität Konstanz M656, D-78457 Konstanz, Germany.

*To whom correspondence should be addressed. E-mail: dimroth@micro.biol.ethz.ch (P.D.); kay.diederichs@uni-konstanz.de (K.D.)

movement of the cytoplasmic against the periplasmic surface of the c ring (fig. S1).

Vonck *et al*. (*13*) determined the position of the periplasmic and the cytoplasmic interfaces of the membrane surrounding the c ring, which are approximately at Tyr^{80} and Ser^{55}, respectively (Fig. 2). On the inner surface of the c ring, near the N- and C-termini, the map shows an extended electron density that can be modeled by an alkyl chain of nine C atoms per c subunit. We propose that detergents are bound here at a position corresponding to that of the external leaflet of the membrane. The Phe^{5} residues at the periplasmic end of the inner surface form a ring that possibly marks the position of the glycerol backbone of phospholipids. Such a positioning of lipids would correlate to the "central plug" feature seen in two-dimensional crystals of c rings (*23*). Despite the lack of direct evidence for a bilayer inside the c ring, its existence can be inferred from the hydrophobic surface that extends beyond the electron density of the alkyl chains until Tyr^{34} (fig. S2B). However, the internal bilayer appears to be wider and shifted toward the periplasmic surface with respect to its external counterpart.

Structure of the sodium ion binding site. The c ring was crystallized in buffer containing 100 mM sodium acetate, which promotes Na^+ binding as shown by established techniques (*15*). The Na^+ ions are seen in the map as 11 distinct densities at the bend of the helices, close to the outer surface of the c ring. Figure 2 shows a section of the c ring with two C-terminal and one N-terminal helix forming a Na^+-binding unit. The coordination sphere is formed by side-chain oxygens of Gln^{32} (Oε1) and Glu^{65} (Oε2) of one subunit and the hydroxyl oxygen of Ser^{66} and the backbone carbonyl oxygen of Val^{63} of the neighboring subunit (Figs. 2 and 3). The distance between the liganding atoms and the ion is 2.37 ± 0.14 Å. The liganding residues are in good accordance with mutational studies, which recognized Gln^{32}, Glu^{65}, and Ser^{66} as being essential for Na^+ binding (*24*), and their arrangement was confirmed as a Na^+ binding site using the algorithm of Nayal and Di Cera (*25*). The crystal structure shows the bound ion surrounded by a network of hydrogen bonds: The Oε1 of Glu^{65} accepts hydrogen bonds from the hydroxyl groups of Ser^{66} and Tyr^{70}, and the Nε2 of Gln^{32} donates a hydrogen bond to Oε2 of Glu^{65} (Fig. 3). These hydrogen bonds serve to keep Glu^{65} deprotonated at physiological pH (*26*) in order to allow Na^+ binding and to lock it into its ion-binding conformation. This arrangement of residues and their hydrogen bonds obviously serves to optimize the solvation energy (*27*) of the Na^+ ion and results in a locked conformation of the ion binding site.

We propose that the present structure with the side chain of Tyr^{70} facing outward and stabilizing the side-chain conformation of Glu^{65} represents the conformation outside of the subunit a/c interface. Toward the periplasmic surface from the binding site, the structure forms a cavity (fig. S2B) to which the side chain of Tyr^{70} could relocate to allow unloading and loading of the binding site to and from subunit a. This relocation may be part of an unlocking mechanism.

The Na^+ binding signature is conserved in all known Na^+-translocating ATP synthases and appears in the c subunits of other an-

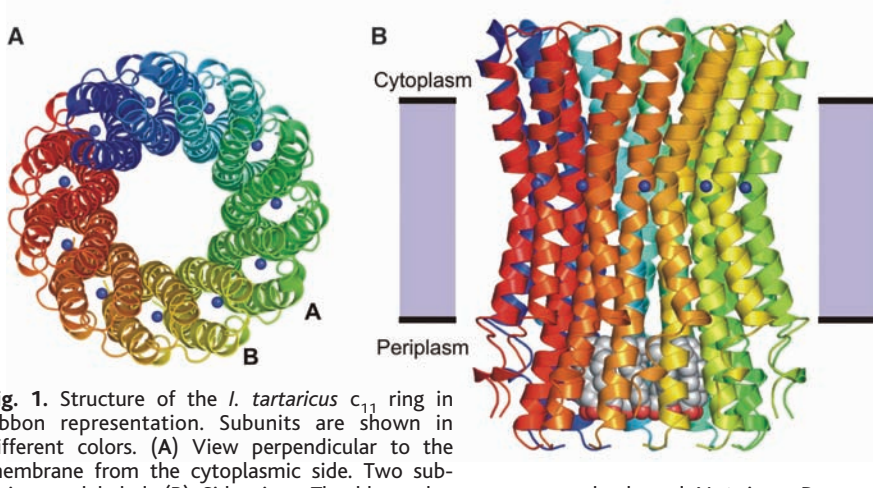

Fig. 1. Structure of the *I. tartaricus* c_{11} ring in ribbon representation. Subunits are shown in different colors. (**A**) View perpendicular to the membrane from the cytoplasmic side. Two subunits are labeled. (**B**) Side view. The blue spheres represent the bound Na^+ ions. Detergent molecules inside the ring are shown with red and gray spheres for clarity. The membrane is indicated as a gray shaded bar (width, 35 Å). The images were created with PyMOL (*36*).

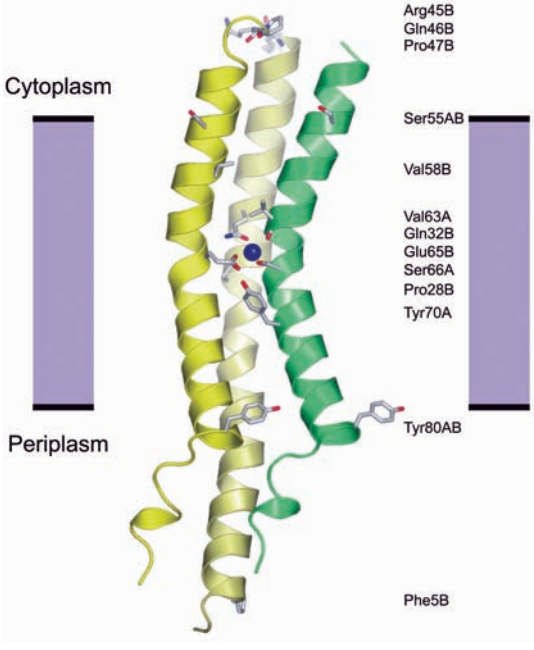

Fig. 2. Section of the c ring showing the interface between the N-terminal and two C-terminal helices with those side chains discussed in the text. This three-helix bundle represents a functional unit responsible for Na^+ binding and allowing access of the ion to the binding site. The view is normal to the external surface of the c ring with the ring axis approximately vertical. The color coding of the subunits is the same as in Fig. 1A.

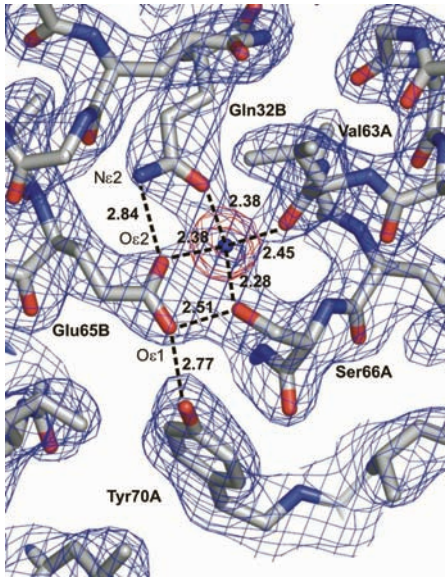

Fig. 3. Electron density map (red, Na^+ omit map at 3.0 σ; blue, $2F_{obs} - F_{calc}$ map at 1.4 σ) and residues of the Na^+ binding site formed by two c subunits, A and B. Na^+ coordination and selected hydrogen bonds are indicated with dashed lines. Distances are given in Å. The blue sphere indicates the center of the bound Na^+ ion. The view is the same as in Fig. 2.

aerobic bacteria, suggesting that they may indeed harbor a Na^+-ATP synthase (Fig. 4). Notably, none of these amino acids are conserved in proton-translocating ATP synthases, except for the acidic residue at position 65 (*I. tartaricus* numbering, Fig. 4), which is implicated in proton binding. Despite these differences in sequence, proton- and Na^+-driven F_o motors must share the same basic structure because of the demonstration that chimeric ATP synthases are functional (*28*).

Ion translocation in F_o complexes. Previous models of the *E. coli* c ring were based on monomeric structures of the c subunit determined by NMR at pH 5 (*11*) and pH 8 (*7*) in solutions using organic solvents and were assumed to represent the protonated and unprotonated structures outside and inside the subunit a/c interface, respectively. In these models, the proton binding Asp^{61} (position 65 in *I. tartaricus*) of those c subunits, which are in contact with the lipids, faces toward the N-terminal helices. Within the subunit a/c interface, the C-terminal helix is proposed to swivel by ~140° clockwise (as viewed from the cytoplasm), which relocates Asp^{61} to become accessible to subunit a (*29*). The latter conformation is supported by cysteine cross-linking in F_o complexes. These experiments indicate that residues at the same helical face as the proton binding site (Ile^{55}, Ala^{62}, Met^{65}, Gly^{69}, Leu^{72}, and Tyr^{73}) are accessible from subunit a and thus must be located on the surface of the c ring (*30*).

In the structure presented here, the placement of the Na^+ binding site near the surface of the c ring between two C-terminal helices allows for ion transfer to and from subunit a after side-chain movements and does not require large rearrangements of the protein backbone. If the structure of the decameric *E. coli* c ring is modeled according to that of *I. tartaricus*, all residue positions that formed cross-links with subunit a are exposed to the surface (fig. S3). We therefore presume that the tertiary fold of the *E. coli* c monomer in the NMR experiments does not match that in the oligomeric c ring, and we note that the compact structure of the c ring would impose severe sterical restraints against the proposed swiveling.

In addition, the known specific reactivity of the ion-binding carboxyl group with the bulky dicyclohexylcarbodiimide (DCCD) could not be explained if the former is occluded between N- and C-terminal helices. With this specificity in mind, we inspected the c-ring surface near Glu^{65}, looking for a DCCD-accessible binding site. A pocket sufficiently large to accommodate binding of bulky organic molecules extends from Glu^{65} to Val^{58} at the ring surface within the interface between an N-terminal and two C-terminal helices (fig. S2A). The pocket is lined by small hydrophobic residues and is open to the membrane from where the hydrophobic DCCD molecule is thought to bind. The pocket might also contribute a binding site for other hydrophobic organic molecules such as the new class of diarylquinoline antibiotics against tuberculosis that target subunit c of *Mycobacterium tuberculosis* (*31*).

To allow for unloading and loading of the ion binding site, the locked conformation must be converted to an open one during passage of the site through the subunit a/c interface. This interconversion may be enabled by modulating the electrostatic interactions of the binding site with the universally conserved Arg^{227} of subunit a (*32*) as the site passes this positively charged residue during rotation (fig. S4).

The path of the ion leading from the binding site into the cytoplasm is presently unknown. Two possibilities are discussed: a channel through subunit a (*10*) or through the c ring itself (*3*). In accord with the latter possibility, biochemical data suggest that the Na^+ exit path is built intrinsically into the c ring (*15*). In the present c-ring structure, a channel leading from the binding site to the cytoplasmic surface could not be identified. Similarly, a channel-like pore is not visible in the structure of the Ca^{2+} ATPase (adenosine triphosphatase), which operates at a rate comparable to that of the ATP synthase (*33*), and in myoglobin (*34*). In contrast to these proteins with a low rate of ion flux, proteins with a structurally evident channel (e.g., potassium channel) have diffusion-limited transport rates up to 10^8 ions per second (*35*), six orders of magnitude faster than the ATP synthase. However, dynamic fluctuations of the protein may open transient pathways for Na^+ conduction so that a wider pore is not evident in the structure.

Taken together, the structural features of ion binding in the membrane-embedded c ring have profound implications for loading and unloading of the binding site because they represent stringent restraints for possible explanations of the F_o motor function.

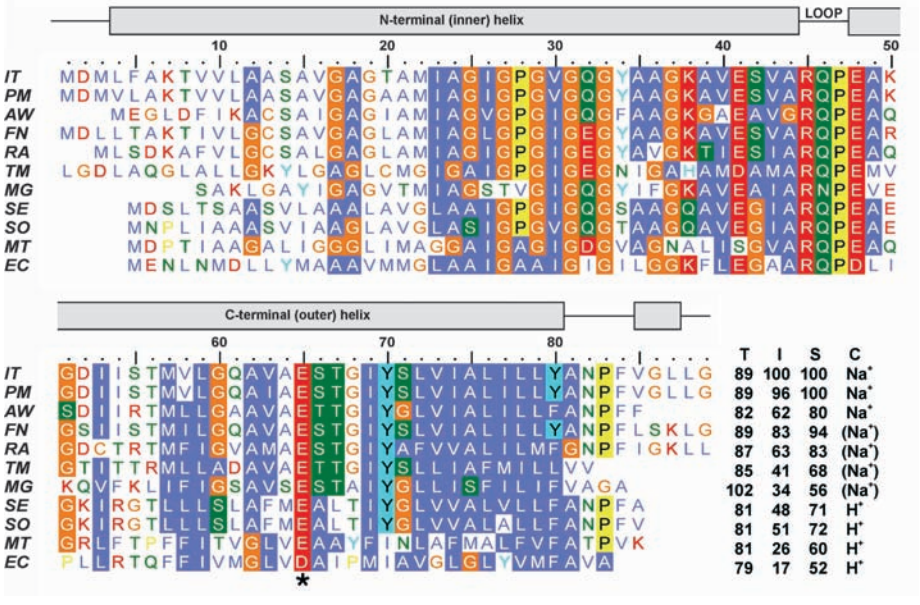

Fig. 4. Alignment of selected c subunit sequences. Amino acids are shaded with a threshold of 70% for identical and similar amino acids among the sequences shown. Orange: G, C; yellow: P; blue: A, V, L, I, M, F, W; green: S, T, N, Q; red: D, E, R, K; cyan: H and Y. Also shown are the total number of amino acids (T), the percentages of identical (I) and similar (S) amino acids (compared with *IT*), and the coupling ion (C) bound to the acidic residue marked by an asterisk. (Na^+) marks putative Na^+-binding c subunits. *I. tartaricus* (*IT*), *Propionigenium modestum* (*PM*), *Acetobacterium woodii c2/3* (*AW*), *Fusobacterium nucleatum* (*FN*), *Ruminococcus albus* (*RA*), *Thermotoga maritima* (*TM*), *Mycoplasma genitalium* (*MG*), *Synechococcus elongatus* (*SE*), *Spinachia oleracea* (*SO*), *Mycobacterium tuberculosis* (*MT*), *Escherichia coli* (*EC*). Secondary-structure elements and numbering according to *IT* are indicated above the sequences.

References and Notes

1. P. D. Boyer, *Annu. Rev. Biochem.* **66**, 717 (1997).
2. R. A. Capaldi, R. Aggeler, *Trends Biochem. Sci.* **27**, 154 (2002).
3. P. Dimroth, C. von Ballmoos, T. Meier, G. Kaim, *Structure* (*Camb.*) **11**, 1469 (2003).
4. J. P. Abrahams, A. G. Leslie, R. Lutter, J. E. Walker, *Nature* **370**, 621 (1994).
5. H. Noji, R. Yasuda, M. Yoshida, K. Kinosita Jr., *Nature* **386**, 299 (1997).
6. J. L. Rubinstein, J. E. Walker, R. Henderson, *EMBO J.* **22**, 6182 (2003).
7. V. K. Rastogi, M. E. Girvin, *Nature* **402**, 263 (1999).
8. J. Xing, H. Wang, C. von Ballmoos, P. Dimroth, G. Oster, *Biophys. J.* **87**, 2148 (2004).
9. A. Aksimentiev, I. A. Balabin, R. H. Fillingame, K. Schulten, *Biophys. J.* **86**, 1332 (2004).
10. B. A. Feniouk *et al.*, *Biophys. J.* **86**, 4094 (2004).
11. M. E. Girvin, V. K. Rastogi, F. Abildgaard, J. L. Markley, R. H. Fillingame, *Biochemistry* **37**, 8817 (1998).
12. D. Stock, A. G. Leslie, J. E. Walker, *Science* **286**, 1700 (1999).
13. J. Vonck *et al.*, *J. Mol. Biol.* **321**, 307 (2002).
14. H. Seelert *et al.*, *Nature* **405**, 418 (2000).
15. T. Meier *et al.*, *J. Mol. Biol.* **325**, 389 (2003).
16. Materials and methods are available as supporting material on *Science* Online.
17. L. C. Storoni, A. J. McCoy, R. J. Read, *Acta Crystallogr. D Biol. Crystallogr.* **60**, 432 (2004).
18. S. D. Watts, Y. Zhang, R. H. Fillingame, R. A. Capaldi, *FEBS Lett.* **368**, 235 (1995).

19. J. Hermolin, O. Y. Dmitriev, Y. Zhang, R. H. Fillingame, *J. Biol. Chem.* **274**, 17011 (1999).
20. S. P. Tsunoda, R. Aggeler, M. Yoshida, R. A. Capaldi, *Proc. Natl. Acad. Sci. U.S.A.* **98**, 898 (2001).
21. W. Junge *et al.*, *FEBS Lett.* **504**, 152 (2001).
22. K. Suhre, Y. H. Sanejouand, *Nucleic Acids Res.* **32**, W610 (2004).
23. T. Meier, U. Matthey, F. Henzen, P. Dimroth, D. J. Müller, *FEBS Lett.* **505**, 353 (2001).
24. G. Kaim, F. Wehrle, U. Gerike, P. Dimroth, *Biochemistry* **36**, 9185 (1997).
25. M. Nayal, E. Di Cera, *J. Mol. Biol.* **256**, 228 (1996).
26. W. R. Forsyth, J. M. Antosiewicz, A. D. Robertson, *Proteins* **48**, 388 (2002).
27. A. Warshel, J. Aqvist, *Annu. Rev. Biophys. Biophys. Chem.* **20**, 267 (1991).
28. G. Kaim, P. Dimroth, *Eur. J. Biochem.* **218**, 937 (1993).
29. R. H. Fillingame, C. M. Angevine, O. Y. Dmitriev, *FEBS Lett.* **555**, 29 (2003).
30. W. Jiang, R. H. Fillingame, *Proc. Natl. Acad. Sci. U.S.A.* **95**, 6607 (1998).
31. K. Andries *et al.*, *Science* **307**, 223 (2005).
32. F. Wehrle, G. Kaim, P. Dimroth, *J. Mol. Biol.* **322**, 369 (2002).
33. C. Toyoshima, M. Nakasako, H. Nomura, H. Ogawa, *Nature* **405**, 647 (2000).
34. H. Frauenfelder, G. A. Petsko, D. Tsernoglou, *Nature* **280**, 558 (1979).
35. D. A. Doyle *et al.*, *Science* **280**, 69 (1998).
36. W. L. DeLano, www.pymol.org (2002).
37. We thank the staff of the Swiss Light Source synchrotron site for support and M. S. Weiss for crystallographic advice. G. Cook and M. Koppenol are acknowledged for reading the manuscript and H.-J. Apell is acknowledged for discussions. This work was supported by the Deutsche Forschungsgemeinschaft (TR SFB 11) and ETH Research Commission. The atomic coordinates and structure factors have been deposited in the Protein Data Bank (accession code 1YCE).

Supporting Online Material
www.sciencemag.org/cgi/content/full/308/5722/659/DC1
Materials and Methods
Figs. S1 to S4
Table S1
References

17 February 2005; accepted 31 March 2005
10.1126/science.1111199

Parietal Lobe: From Action Organization to Intention Understanding

Leonardo Fogassi,[1,2]* Pier Francesco Ferrari,[2] Benno Gesierich,[2] Stefano Rozzi,[2] Fabian Chersi,[2] Giacomo Rizzolatti[2]

Inferior parietal lobule (IPL) neurons were studied when monkeys performed motor acts embedded in different actions and when they observed similar acts done by an experimenter. Most motor IPL neurons coding a specific act (e.g., grasping) showed markedly different activations when this act was part of different actions (e.g., for eating or for placing). Many motor IPL neurons also discharged during the observation of acts done by others. Most responded differentially when the same observed act was embedded in a specific action. These neurons fired during the observation of an act, before the beginning of the subsequent acts specifying the action. Thus, these neurons not only code the observed motor act but also allow the observer to understand the agent's intentions.

The posterior part of the parietal lobe has been traditionally considered as a typical association cortex. In this view, in the posterior parietal cortex, afferents from two or more sensory channels integrate, and this multimodal sensory association is the basis for some types of percepts, such as space. However, the works of Mountcastle (*1*) and Hyvärinen (*2*), and subsequent studies carried out in several laboratories (*3*–*7*), showed that the posterior parietal cortex, besides "putting together" different sensory modalities (association function), also codes motor actions and provides the representations of these motor actions with specific sensory information. This view stresses the importance of sensorimotor integration in the emergence of perception.

Recently, we reexamined the functional properties of the convexity of IPL (PF/PFG complex) in monkeys, testing the activity of single neurons in response to sensory stimuli and during monkey's active movements (*8*). As previously reported (*2*), we found that IPL convexity has a motor somatotopic organization. Most interestingly, we found that many IPL neurons discharge both when the monkey performs a given motor act and when it observes a similar motor act done by another individual; these neurons are known as parietal mirror neurons (*9*–*11*). Here, we present data on the motor organization of IPL and on its mirror properties.

The coding of motor acts in the inferior parietal lobule. Neurons were recorded from the rostral sector of IPL (Fig. 1A) in two monkeys. All studied neurons (n = 165) were active in association with grasping movements of the hand (grasping neurons). They were formally tested in two main conditions. In the first condition, the monkey, starting from a fixed position (Fig. 1B, left), reached for and grasped a piece of food located in front of it and brought the food to the mouth (Fig. 1B, right, I). In the second condition, the monkey reached for and grasped an object, located as described above, and placed it into a container (Fig. 1B, right, II). In the first condition, the monkey ate the food brought to the mouth; in the second it was rewarded after correct accomplishment of the task.

Although some neurons discharged with the same strength regardless of the motor act that followed grasping, the large majority were influenced by the subsequent motor act. Examples are shown in Fig. 1C. Unit 67 discharged during grasping when grasping was followed by bringing the food to the mouth. In contrast, its discharge was virtually absent when grasping was followed by placing. Unit 161 exemplifies the opposite behavior. This neuron discharged very strongly when grasping was followed by placing, whereas only a weak discharge was present when grasping was followed by bringing to the mouth. Finally, Unit 158 did not show any significant difference in discharge intensity in the two conditions.

Table 1A summarizes the behavior of all recorded neurons. About two-thirds of neurons discharged preferentially ($P < 0.05$) when grasping was embedded into a specific motor action (*12*). The neuron selectivity remained unmodified when the conditions were blocked, as in Fig. 1, or interleaved (fig. S1).

Figure 1D shows the intensity and time course of neuron discharge of the grasp-to-eat and grasp-to-place populations in the two basic conditions. The population analysis (*12*), based on all selective neurons recorded from monkey M2, confirmed the data observed in individual neurons.

To control for the possibility that the differential discharge of neurons during the same motor act could be due to differences in the stimuli that the monkeys grasped, monkeys were trained to grasp an identical piece of food in both conditions. Food placing was achieved by showing the monkey a piece of food that the monkey particularly liked before each trial. After correct placing, the monkey received the preferred food. Unit 122 (Fig. 2) demonstrates that neuron selectivity did not depend on the stimulus used. The same result was found in all tested neurons (n = 28), regardless of whether they coded grasping to eat (n = 22) or grasping to place (n = 6) (*12*).

It is well known from human studies that the first motor act of an action is influenced by the next acts of that action (*13*). We also found that reaching-to-grasp movement followed by arm flexion (bringing the food to

[1]Dipartimento di Psicologia, Università di Parma, Borgo Carissimi 10, 43100 Parma, Italy. [2]Dipartimento di Neuroscienze, Università di Parma, via Volturno 39, 43100 Parma, Italy.

*To whom correspondence should be addressed. E-mail: fogassi@unipr.it